

Measurement of energy correlators inside jets and determination of the strong coupling $\alpha_S(m_Z)$

—Supplemental Material—

Additional figures of the measured E2C and E3C, and their ratio distributions in the eight p_T regions of the analysis, the statistical covariance matrices of the measurements, and the χ^2 values as a function of $\alpha_S(m_Z)$.

The CMS Collaboration

CERN

(Dated: June 23, 2024)

Energy correlators that describe energy-weighted distances between two or three particles in a hadronic jet are measured using an event sample of $\sqrt{s} = 13$ TeV proton-proton collisions collected by the CMS experiment and corresponding to an integrated luminosity of 36.3 fb^{-1} . The measured distributions are consistent with the trends in the simulation that reveal two key features of the strong interaction: confinement and asymptotic freedom. By comparing the ratio of the measured three- and two-particle energy correlator distributions with theoretical calculations that resum collinear emissions at approximate next-to-next-to-leading logarithmic accuracy matched to a next-to-leading order calculation, the strong coupling is determined at the Z boson mass: $\alpha_S(m_Z) = 0.1229^{+0.0049}_{-0.0050}$, the most precise $\alpha_S(m_Z)$ value obtained using jet substructure observables.

Figures 1 and 2 show the measured (unfolded) E2C and E3C distributions, compared to various MC predictions in the eight p_T regions of the analysis. The MC predictions include PYTHIA8.240 using [1] and [2] showers, with the CP5 tune; HERWIG7.1.4 using dipole showers, with the CH3 tune; and SHERPA2.2 [3], with its default tune. The value of $\alpha_S(m_Z)$ is set to 0.118, with its energy evolution computed at two-loop order. The E3C/E2C ratios are compared with MC predictions in Fig. 3 and with theoretical predictions in Fig. 4. The χ^2 values determined from the fit of measured data as a function of $\alpha_S(m_Z)$ are shown in Fig. 5. The statistical correlation matrices of the unfolded E2C and E3C distributions, and of their

ratio, are shown in Figs. 6–8.

-
- [1] N. Fischer, S. Prestel, M. Ritzmann, and P. Skands, for hadron colliders, Eur. Phys. J. C **76**, 589 (2016).
 - [2] S. Höche and S. Prestel, The midpoint between dipole and parton showers, Eur. Phys. J. C **75**, 461 (2015).
 - [3] E. Bothmann *et al.* (Sherpa), Event generation with SHERPA 2.2, SciPost Phys. **7**, 034 (2019).
 - [4] W. Chen, J. Gao, Y. Li, Z. Xu, X. Zhang, and H. X. Zhu, NNLL resummation for projected three-point energy correlator (2023).

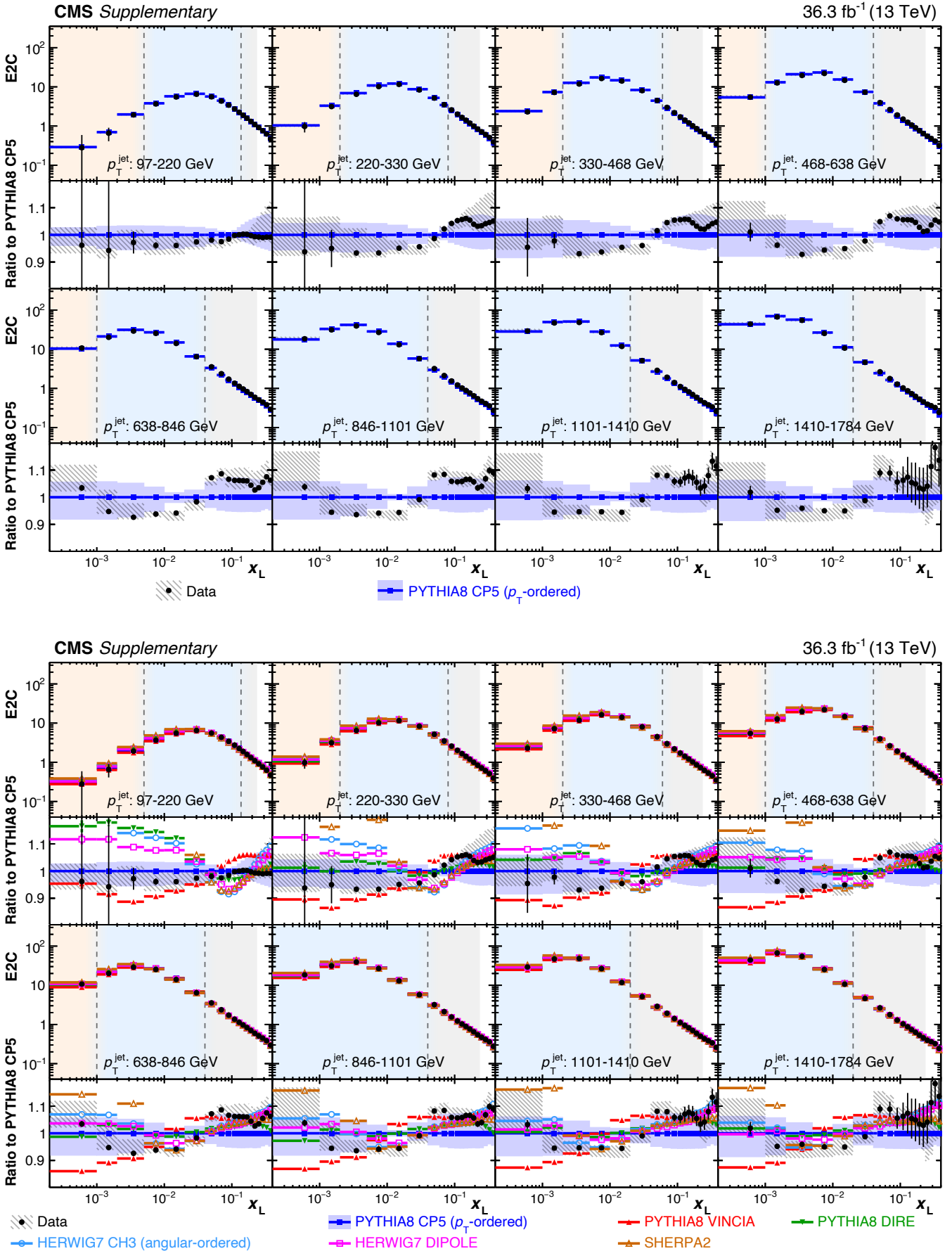


FIG. 1. Measured (unfolded) E2C distributions compared with the PYTHIA8 CP5 prediction (upper) and all the MC predictions (lower) in the eight p_T regions. Statistical and experimental systematic uncertainties are shown with error bars and hatched bands, respectively. The theory uncertainty in the PYTHIA8 CP5 prediction is shown with the blue bands.

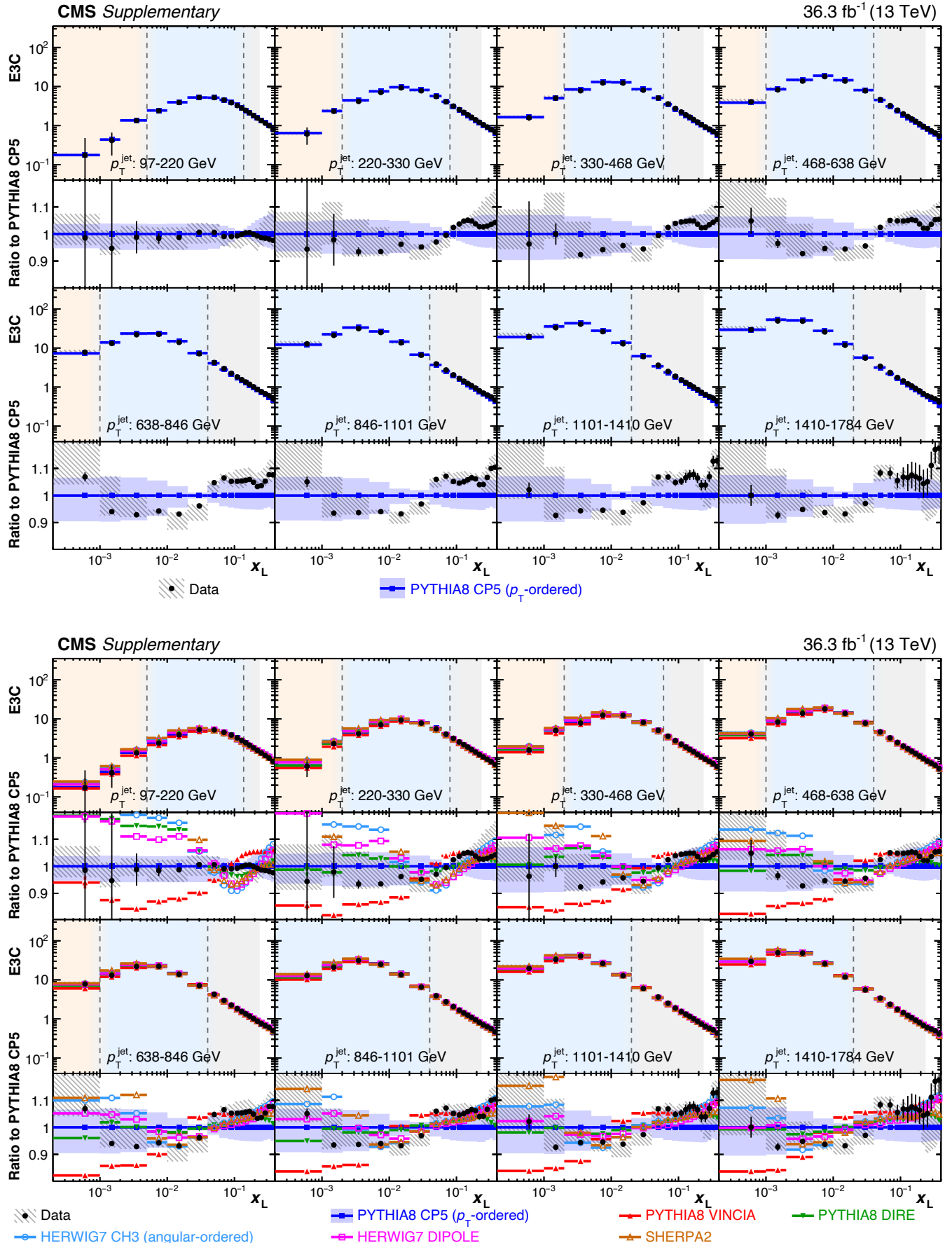


FIG. 2. Measured (unfolded) E3C distributions compared with the PYTHIA8 CP5 prediction (upper) and all the MC predictions (lower) in the eight p_T regions. Statistical and experimental systematic uncertainties are shown with error bars and hatched bands, respectively. The theory uncertainty in the PYTHIA8 CP5 prediction is shown with the blue bands.

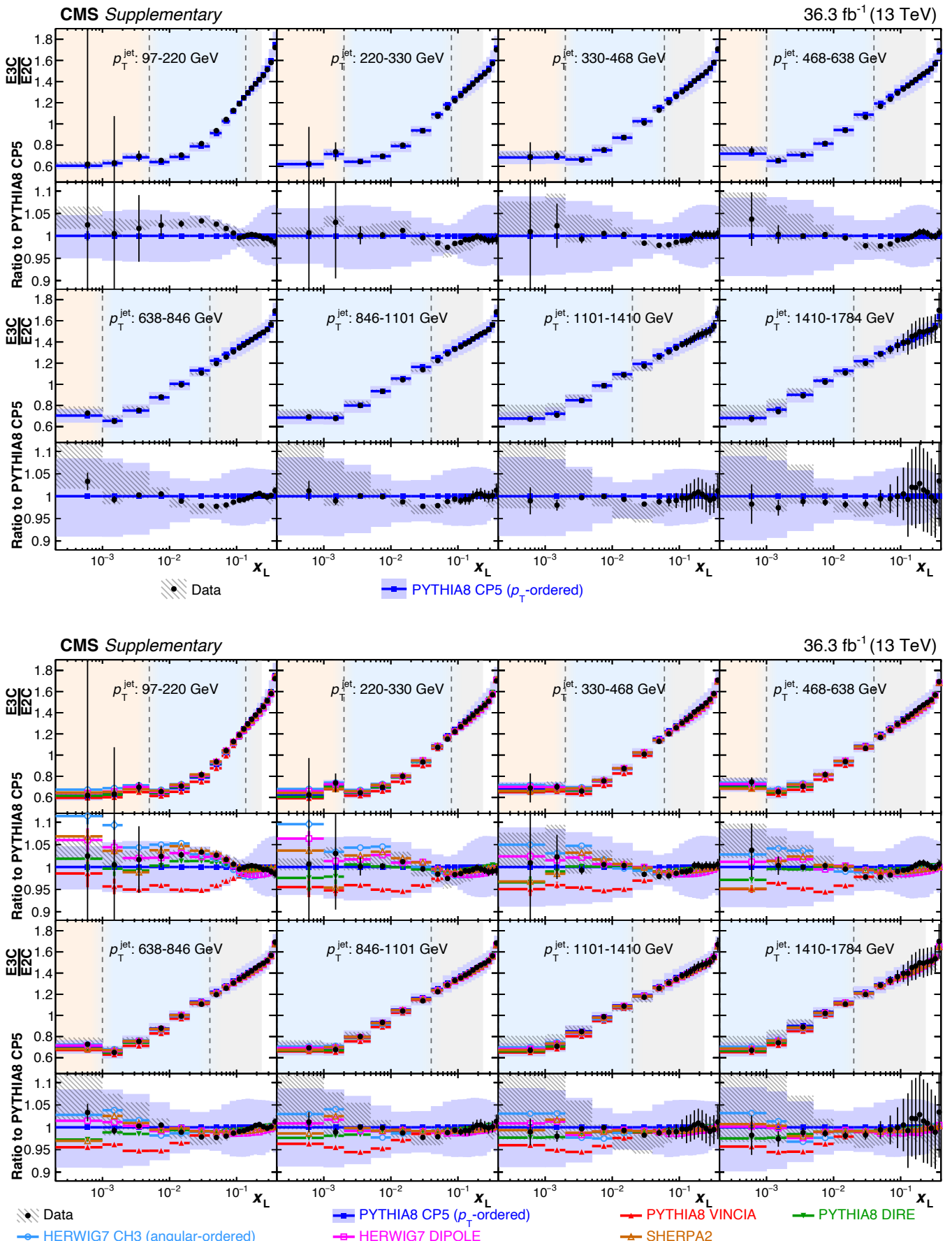


FIG. 3. Ratio of the unfolded E3C and E2C distributions compared with the PYTHIA8 CP5 prediction (upper) and all the MC predictions (lower) in the eight p_T regions. Statistical and experimental systematic uncertainties are shown with error bars and hatched bands, respectively. The theory uncertainty in the PYTHIA8 CP5 prediction is shown with the blue bands.

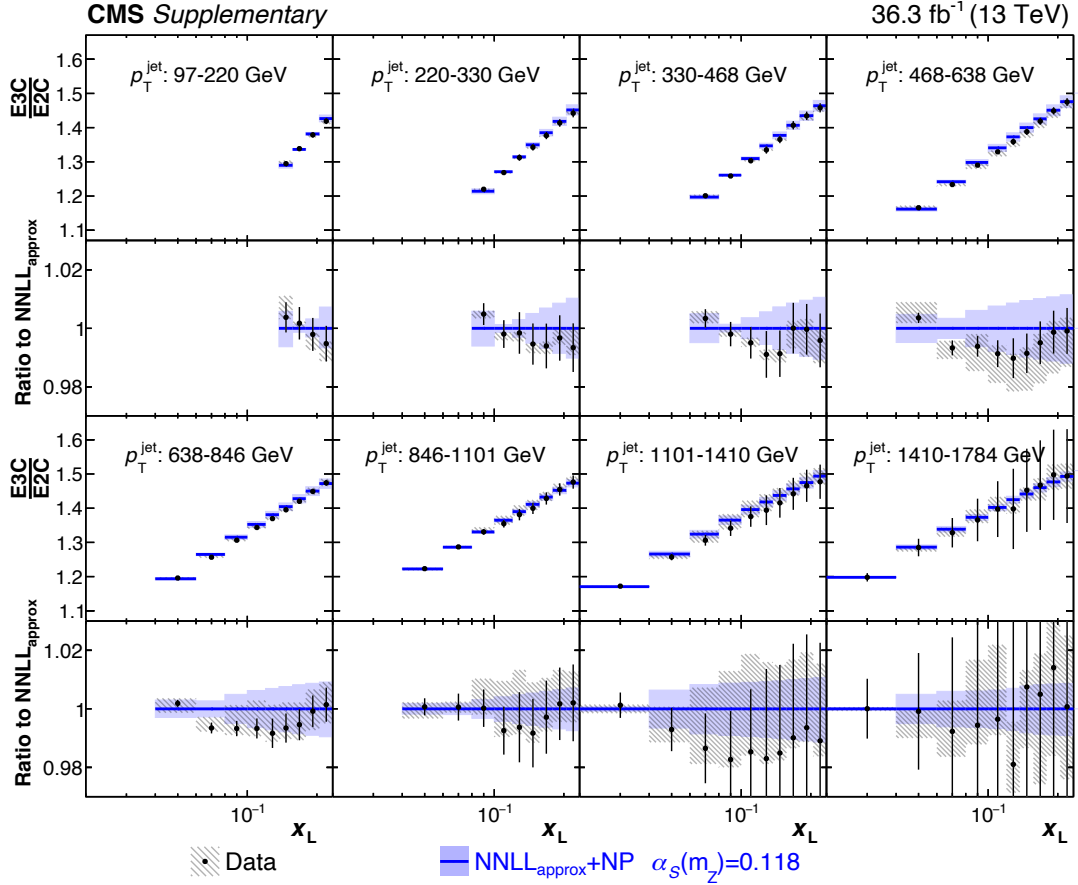


FIG. 4. Ratio of the unfolded E3C and E2C distributions in the eight p_T regions. The NLO + NNLL_{approx} theoretical predictions [4] and the corresponding uncertainties are corrected to hadron-level and normalized to the measured data. The statistical and experimental systematic uncertainties are shown with error bars and boxes, respectively.

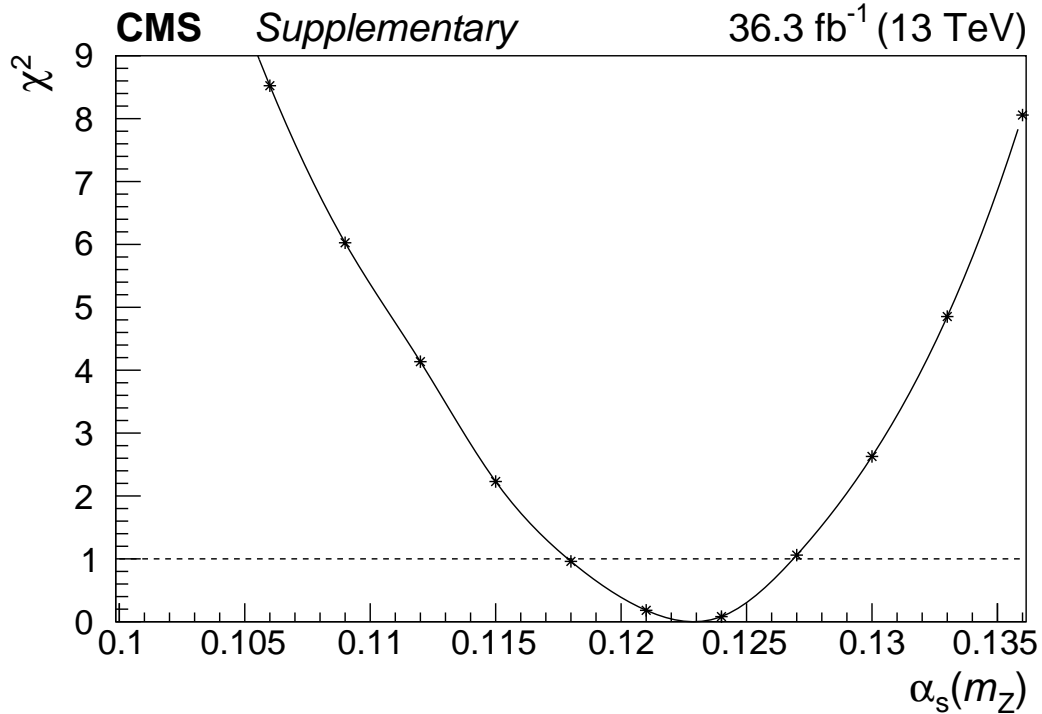


FIG. 5. The χ^2 values determined from the fit of the measured data, as a function of $\alpha_s(m_Z)$.

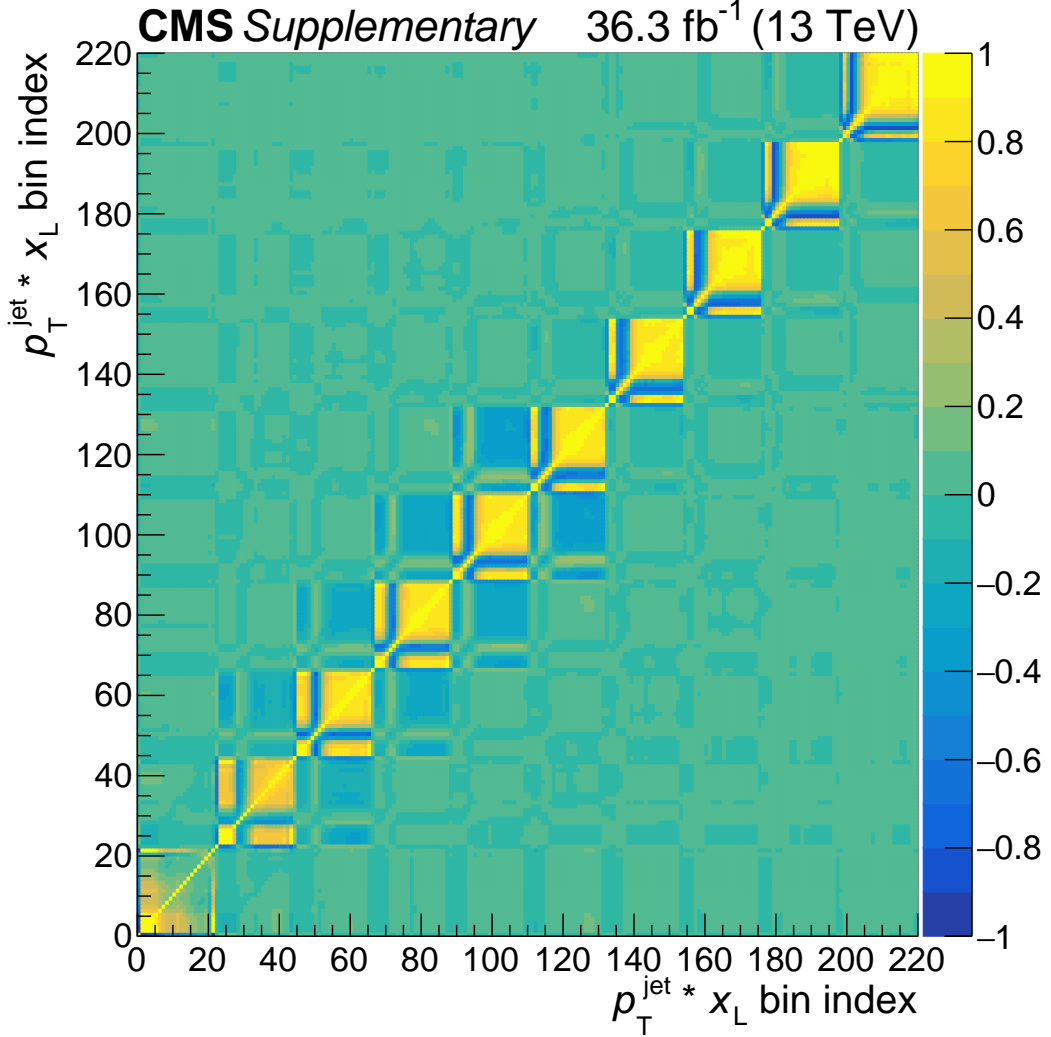


FIG. 6. The statistical correlation matrix of the bins of the unfolded E2C distribution. The bin number n in this figure is defined by $n = 22i_{p_T} + i_{x_L}$, where i_{p_T} and i_{x_L} are the indices of the p_T and x_L bins. In total there are ten p_T bins, the eight presented in the analysis plus the overflow and underflow bins. The number of x_L bins per p_T region is 22.

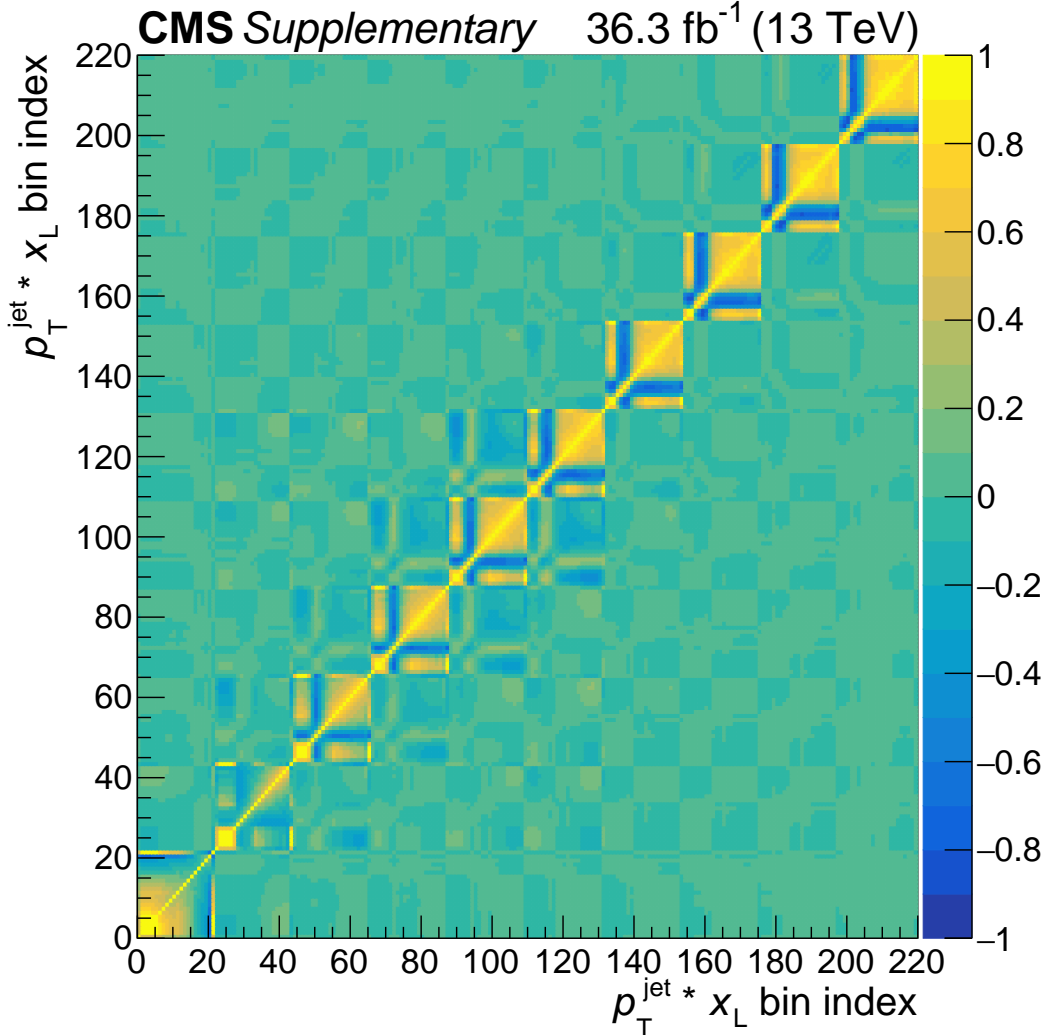


FIG. 7. The statistical correlation matrix of the bins of the unfolded E3C distribution. The bin number n in this figure is defined by $n = 22i_{p_T} + i_{x_L}$, where i_{p_T} and i_{x_L} are the indices of the p_T and x_L bins. In total there are ten p_T bins, the eight presented in the analysis plus the overflow and underflow bins. The number of x_L bins per p_T region is 22.

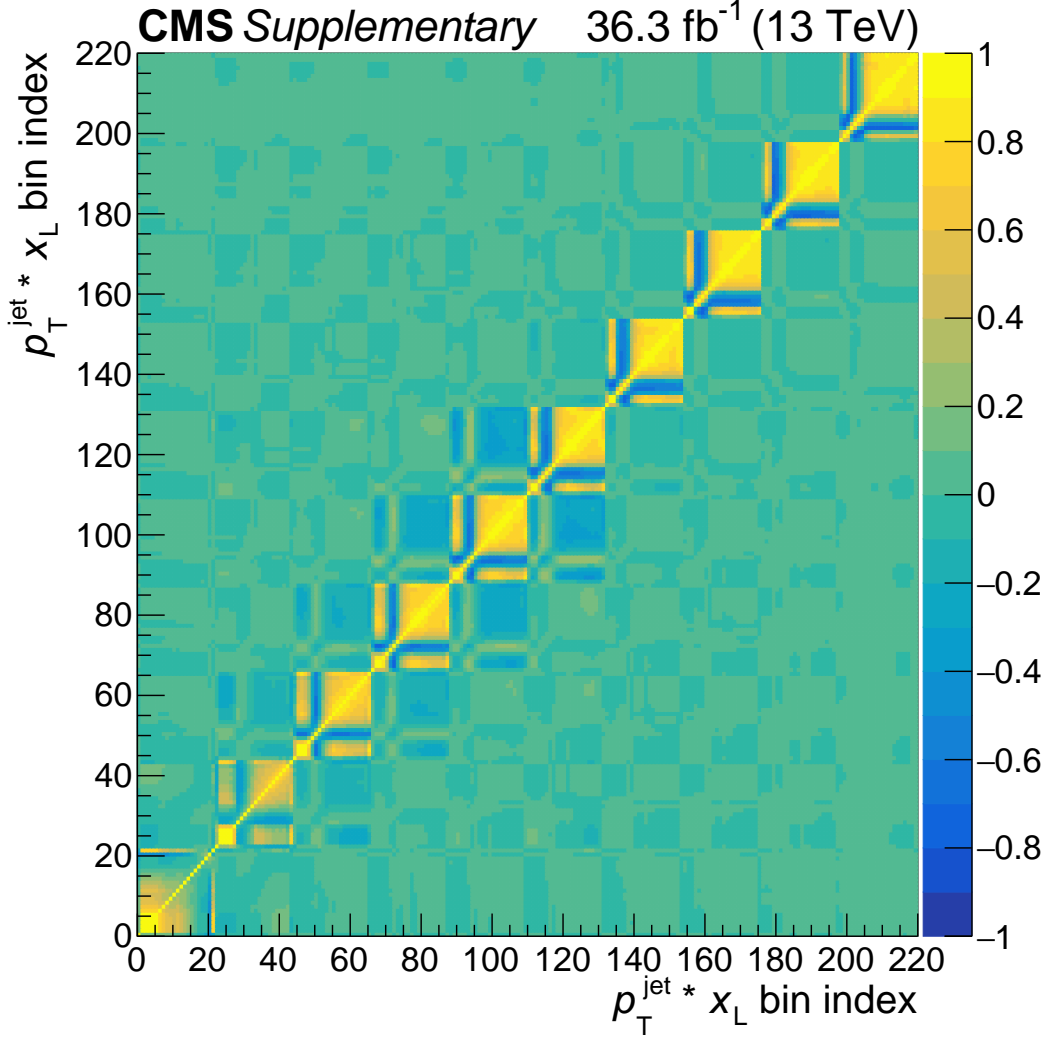


FIG. 8. The statistical correlation matrix of the bins of the unfolded E3C/E2C distribution. The bin number n in this figure is defined by $n = 22i_{p_T} + i_{x_L}$, where i_{p_T} and i_{x_L} are the indices of the p_T and x_L bins. In total there are ten p_T bins, the eight presented in the analysis plus the overflow and underflow bins. The number of x_L bins per p_T region is 22.